Localized Surface Plasmon Resonance Spectroscopy near Molecular Resonances

Amanda J. Haes,[§] Shengli Zou, Jing Zhao, George C. Schatz,* and Richard P. Van Duyne*

Contribution from the Department of Chemistry, Northwestern University, Evanston, Illinois 60208-3113

Received May 22, 2006; E-mail: vanduyne@chem.northwestern.edu; schatz@chem.northwestern.edu

Abstract: The peak location of the localized surface plasmon resonance (LSPR) of noble metal nanoparticles is highly dependent upon the refractive index of the nanoparticles' surrounding environment. In this study, new phenomena are revealed by exploring the influence of interacting molecular resonances and nanoparticle resonances. The LSPR peak shift and line shape induced by a resonant molecule vary with wavelength. In most instances, the oscillatory dependence of the peak shift on wavelength tracks with the wavelength dependence of the real part of the refractive index, as determined by a Kramers–Kronig transformation of the molecular resonance absorption spectrum. A quantitative assessment of this shift based on discrete dipole approximation calculations shows that the Kramers–Kronig index must be scaled in order to match experiment.

Introduction

The effect molecules have on the intrinsic properties of noble metal and metal oxide thin films and nanoparticles is an active area of research. This has been driven, in part, by the interest in understanding surface-enhanced spectroscopies.[1–5] Of the many surface-enhanced spectroscopies, surface-enhanced Raman scattering (SERS) is the most widely used technique. When a Raman-active molecule is placed near a roughened noble metal surface, the electromagnetic fields induce a dipole in the molecule, resulting in an enhancement over the normal Raman signal.[6] If the molecule probed contains a molecular resonance that overlaps with the laser excitation (termed surface-enhanced resonance Raman spectroscopy (SERRS)), additional orders of magnitude in signal intensity can be gained.[5] These techniques provide enough sensitivity to allow the detection of single molecules.[7,8] While the cause of these observations is not fully understood,[2] there is a large amount of evidence that suggests that the optical properties of the metal substrate and the electronic transitions of the molecule (or its byproducts) play an important role in the mechanistic understanding with all SERS experiments.

A different but related approach to study the influence of molecules on the optical response of nanoparticles is localized surface plasmon resonance (LSPR) spectroscopy, an effective platform that detects refractive index changes near the surfaces of noble metal nanoparticles.[9–16] The LSPR phenomenon arises when a resonance condition between the incident wavelength of light and the electrons in the nanoparticles is met. This causes a collective oscillation of the conduction electrons in the nanoparticles and has two primary consequences. First, the wavelengths of light that cause this collective oscillation are selectively absorbed by the nanoparticles and can be monitored using ultraviolet–visible (UV–vis) spectroscopy.[17] The second consequence is the formation of enhanced electromagnetic fields that extend from the nanoparticle surfaces. These fields are responsible for a large portion of the enhancement observed in all surface-enhanced spectroscopies.

Recently, it has been demonstrated that Ag nanotriangles fabricated by nanosphere lithography (NSL) function as extremely sensitive chemical and biological optical nanosensors by monitoring adsorbate-induced wavelength shifts in the LSPR peak extinction.[9,12,13,18] NSL has proven to be a nearly ideal

§ Current address: University of Iowa, Iowa City, IA.

(1) Schatz, G. C.; Van Duyne, R. P. *Electromagnetic Mechanism of Surface-Enhanced Spectroscopy*; Wiley: New York, 2002; Vol. 1.
(2) Andersen, P. C.; Jacobson, M. L.; Rowlen, K. L. *J. Phys. Chem. B* **2004**, *108*, 2148–2153.
(3) Geddes, C. D.; Parfenov, A.; Roll, D.; Fang, J.; Lakowicz, J. R. *Langmuir* **2003**, *19*, 6236–6241.
(4) Etchegoin, P.; Cohen, L. F.; Hartigan, H.; Brown, R. J. C.; Milton, M. J. T.; Gallop, J. C. *Chem. Phys. Lett.* **2004**, *383*, 577–583.
(5) Haynes, C. L.; Van Duyne, R. P. *J. Phys. Chem. B* **2003**, *107*, 7426–7433.
(6) Jeanmaire, D. L.; Van Duyne, R. P. *J. Electroanal. Chem. Interfacial Electrochem.* **1977**, *84*, 1–20.
(7) Nie, S.; Emory, S. R. *Science* **1997**, *275*, 1102–1106.
(8) Kneipp, K.; Wang, Y.; Kneipp, H.; Perelman, L. T.; Itzkan, I.; Dasari, R. R.; Feld, M. S. *Phys. Rev. Lett.* **1997**, *78*, 1667–1670.

(9) Malinsky, M. D.; Kelly, K. L.; Schatz, G. C.; Van Duyne, R. P. *J. Am. Chem. Soc.* **2001**, *123*, 1471–1482.
(10) Haes, A. J.; Zou, S.; Schatz, G. C.; Van Duyne, R. P. *J. Phys. Chem. B* **2004**, *108*, 109–116.
(11) Haes, A. J.; Zou, S.; Schatz, G. C.; Van Duyne, R. P. *J. Phys. Chem. B* **2004**, *108*, 6961–6968.
(12) Haes, A. J.; Van Duyne, R. P. *J. Am. Chem. Soc.* **2002**, *124*, 10596–10604.
(13) Riboh, J. C.; Haes, A. J.; McFarland, A. D.; Yonzon, C. R.; Van Duyne, R. P. *J. Phys. Chem. B* **2003**, *107*, 1772–1780.
(14) McFarland, A. D.; Van Duyne, R. P. *Nano Lett.* **2003**, *3*, 1057–1062.
(15) Nath, N.; Chilkoti, A. *Proc. SPIE* **2002**, *4626*, 441–448.
(16) Nath, N.; Chilkoti, A. *Anal. Chem.* **2002**, *74*, 504–509.
(17) Jensen, T. R.; Malinsky, M. D.; Haynes, C. L.; Van Duyne, R. P. *J. Phys. Chem. B* **2000**, *104*, 10549–10556.
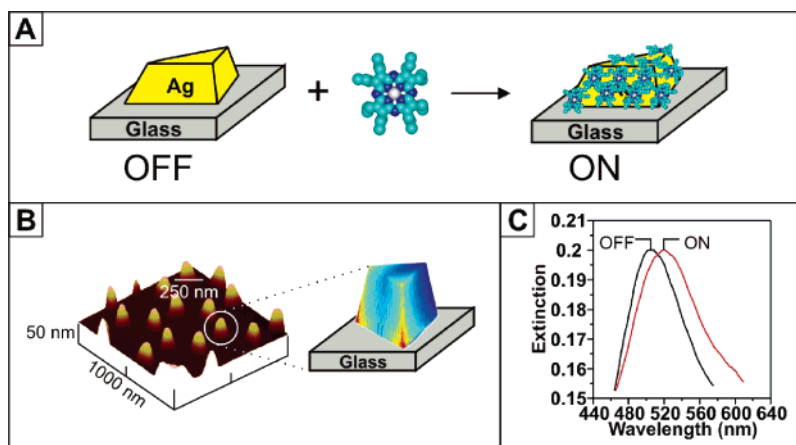(18) Haes, A. J.; Van Duyne, R. P. *Mater. Res. Soc. Symp. Proc.* **2002**, *723*, O3.1.1–O3.1.6.

Figure 1. (A) Schematic illustration of the interacting molecular resonance of [2,3,7,8,12,13,17,18-octakis(propyl)porphyrazinato]magnesium(II) (MgPz) and Ag nanoparticle LSPR system. MgPz was determined to lie flat on the nanoparticles via AFM. (B) A three-dimensional AFM image of the triangular silver nanoparticles used in the experiments and an electrodynamic model of a silver nanoparticle. (C) Representative LSPR spectra representing the nanoparticle LSPR before (OFF) and after (ON) incubation in MgPz.

nanofabrication tool for these studies because it can produce surface-confined nanoparticles with fixed interparticle spacings in a massively parallel manner. Because NSL-derived nanoparticles do not aggregate, they behave optically as *N* weakly coupled nanoparticles rather than as an array of strongly coupled nanoparticles; thus, NSL-derived nanoparticles permit us to focus on adsorbate-induced local refractive index changes and/or charge-transfer interactions independent of aggregation-mediated optical responses. Furthermore, NSL allows for the easy manipulation of the LSPR extinction peak maximum location (λ_{max}) by varying the nanoparticle size, shape, and composition.[19,20]

To date, all LSPR sensing experiments have been performed with electronically nonresonant adsorbates.[9–14] In these experiments, it was assumed that the electronic structure of the molecules did not change during the course of these experiments and did not influence the signal transduction in the sensing events. However, since many biomolecules contain visible chromophores, it is important to understand the influence that electronic transitions will have on biosensing events. Additionally, the interaction between the LSPR of noble metal nanoparticles and molecular resonances has implications in understanding SERRS. Recent results indicate that molecular resonances do not damp the LSPR of NSL-prepared nanoparticle substrates and give rise to SERS enhancement factors ~40 times larger than those obtained in studies in which nonresonant enhanced SERS samples are interrogated.[5] Although some of the fundamental theory describing the interaction of a resonant molecule with a metal particle is quite old,[21] the influence of this interaction on wavelengths shifts has not been studied.

Recently, propagating surface plasmon resonance (SPR) spectroscopy, a refractive-index-based sensing technique that relies on the propagation of electromagnetic waves along the surface of a metal film, has been used to study the interaction of resonant molecules with the enhanced fields. Several groups demonstrated that molecules containing electronic transitions have a large influence in the signal response in SPR experi-

ments.[22–29] In all cases, it was concluded that the response of the sensor depended strongly on the wavelength-dependent change in the real part of the adsorbate's refractive index.

In this study, the effect of interacting molecular resonances and nanoparticle-localized surface plasmon resonances is studied. NSL is used to fabricate Ag nanoparticles with a range of sizes and shapes such that the LSPR peak wavelength is tuned through the molecular resonance spectrum. A schematic representation of the experiment can be found in Figure 1. Adding the adsorbate layer leads to a shift ($\Delta\lambda_{max}$) in the plasmon wavelength, as well as changes in the full width at half-maximum (FWHM) and intensity of the LSPR peak. To interpret the results, we perform a Kramers–Kronig analysis to determine the wavelength-dependent refractive index of the adsorbate. This result is then used in finite element electrodynamics calculations using the discrete dipole approximation to provide a direct simulation of the measurements. The refractive index can also be used to provide an empirical prediction of the wavelength dependence of the LSPR shift ($\Delta\lambda_{max}$), and this matches at least qualitatively with experiment. However, our quantitative assessment shows that the Kramers–Kronig result needs to be scaled in order to match experiment. We anticipate that these findings will substantially influence the optimization of refractive-index-based sensing of biomolecules with resonant chromophores and contribute to the overall understanding of surface-enhanced spectroscopies.

Experimental Methods

Materials. Absolute ethanol was obtained from Pharmco (Brookfield, CT). Methanol and hexanes were purchased from Fisher Scientific (Pittsburgh, PA). Silver wire (99.99%, 0.5 mm diameter) was purchased from D.F. Goldsmith (Evanston, IL). Tungsten vapor deposition boats

(19) Hulteen, J. C.; Van Duyne, R. P. *J. Vac. Sci. Technol. A* **1995**, *13*, 1553–1558.
(20) Haynes, C. L.; Van Duyne, R. P. *J. Phys. Chem. B* **2001**, *105*, 5599–5611.
(21) Gersten, J.; Nitzan, A. *J. Chem. Phys.* **1980**, *73*, 3023–3037.

(22) Kurihara, K.; Nakamura, K.; Hirayama, E.; Suzuki, K. *Anal. Chem.* **2002**, *74*, 6323–6333.
(23) Kurihara, K.; Suzuki, K. *Anal. Chem.* **2002**, *74*, 696–701.
(24) Wang, S.; Boussaad, S.; Tao, N. J. *Surfact. Sci. Ser.* **2003**, *111*, 213–251.
(25) Wang, S.; Boussaad, S.; Wong, S.; Tao, N. J. *Anal. Chem.* **2000**, *72*, 4003–4008.
(26) Boussaad, S.; Pean, J.; Tao, N. J. *Anal. Chem.* **2000**, *72*, 222–226.
(27) Zangeneh, M.; Doan, N.; Sambriski, E.; Terrill, R. H. *Appl. Spectrosc.* **2004**, *58*, 10–17.
(28) Pockrand, I.; Brillante, A.; Mobius, D. *J. Chem. Phys.* **1982**, *77*, 6289–6295.
(29) Pockrand, I.; Swalen, J. D.; Gordon, J. G.; Philpott, M. R. *J. Chem. Phys.* **1979**, *70*, 3401–3408.

were acquired from R.D. Mathis (Long Beach, CA). Polystyrene nanospheres with diameters of 280 ± 4, 310 ± 9, 390 ± 19.5, 400 ± 8, 450 ± 5, and 510 ± 11 nm were received as a suspension in water (Interfacial Dynamics Corp., Portland, OR, or Duke Scientific, Palo Alto, CA) and were used without further treatment. Millipore cartridges (Marlborough, MA) were used to purify water to a resistivity of 18.2 $M\Omega \cdot cm^{-1}$. Fisherbrand No. 2 glass coverslips with 18 mm diameters were obtained from Fisher Scientific. [2,3,7,8,12,13,17,18-Octakis-(propyl)porphyrazinato]magnesium(II) (MgPz) was received as a gift from Brian Hoffman's group (Northwestern University). $Fe(NH_4)_2SO_4 \cdot 6H_2O$, 2,2′-dipyridyl, and NH_4PF_6 were obtained from Sigma Aldrich (St. Louis, MO).

Substrate Preparation. Glass substrates were cleaned in piranha solution (1:3 30% H_2O_2/H_2SO_4) for 30 min at 80 °C. (***Warning:** Piranha reacts violently with organic compounds and should be handled with caution!*) Samples were allowed to cool and were then rinsed profusely with water. Samples were then sonicated in 5:1:1 $H_2O/NH_4OH/30\%$ H_2O_2 and rinsed with water. The samples were stored in ultrapure water prior to use.

Nanoparticle Preparation. NSL was used to create monodisperse, surface-confined Ag nanotriangles.[10,12] Polystyrene nanospheres (~2.2 μL) were drop-coated onto the glass substrates and allowed to dry, forming a monolayer in a close-packed hexagonal formation, which served as a deposition mask. The samples were mounted into a Consolidated Vacuum Corp. vapor deposition chamber. A Leybold Inficon XTM/2 quartz crystal microbalance (East Syracuse, NY) was used to measure the thickness of the Ag film deposited over the nanosphere mask, d_m. Following metal deposition, the samples were sonicated for 3−5 min in ethanol to the remove the polystyrene nanosphere mask. The perpendicular bisector of the nanoparticles, a, was varied by changing the diameter, D, of the nanospheres used. The height of the nanoparticles, b, was varied by depositing varying amounts of Ag onto the sample. These two parameters were varied to alter the LSPR peak position throughout the visible region of the spectrum.

Nanoparticle Solvent Annealing and Functionalization. Immediately following nanosphere removal, the samples were placed in hexanes to induce long-term stability of the optical properties of the nanoparticles. For each experiment, the sample was stabilized and functionalized in a home-built flow cell.[9] Prior to modification, the Ag nanoparticles were solvent-annealed[9] with hexanes and methanol. Dry N_2 gas and solvent were cycled through the flow cell until the λ_{max} of the sample stabilized. Samples were then incubated in 100 μM Fe(bpy)$_3^{2+}$ or 50 μM MgPz ethanolic solutions for 30 min or 1 h, respectively. These times were determined to produce repeatable and approximately full monolayer coverages of the given analyte (data not shown). After incubation, the nanoparticle samples were rinsed with 10−20 mL of ethanol and dried by flowing N_2 gas through the sample cell.

Ultraviolet−Visible Extinction Spectroscopy. Macroscale UV−vis extinction measurements were collected using an Ocean Optics (Dunedin, FL) SD2000 or HR2000 fiber-optic coupled spectrometer with a charge-coupled device (CCD) detector. All spectra in this study are macroscopic measurements performed in standard transmission geometry with unpolarized light. The probe diameter was approximately 2 mm.

Ultraviolet−Visible Surface Absorption Spectroscopy of MgPz. UV−vis measurements of the surface absorption MgPz to thin metal films were collected using an integrating sphere (LabSphere) and fiber-optic coupled spectrometer (USB2000-VIS-NIR, Ocean Optics) with a CCD detector. MgPz (50 μM in ethanol) was adsorbed onto a 200 nm thick Ag film (vapor-deposited onto a glass substrate) by immersion at room temperature for 12 h, followed by rinsing in ethanol. Two reflectance spectra were measured. The reference spectrum, reference-(λ), was that of an identical 200 nm thick Ag film on glass with no MgPz adsorbed. The sample spectrum, sample(λ), was that of MgPz on a 200 nm thick Ag film. The surface absorption spectrum was then
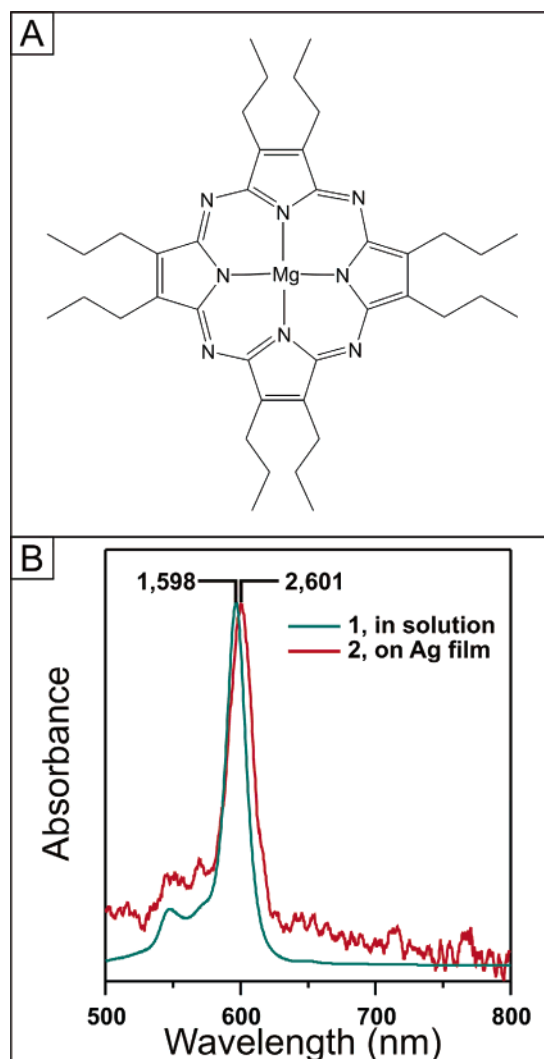

Figure 2. [2,3,7,8,12,13,17,18-Octakis(propyl)porphyrazinato]magnesium-(II). (A) Structure of [2,3,7,8,12,13,17,18-octakis(propyl)porphyrazinato]-magnesium(II) (MgPz) (MW = 673.24 g/mol, $\epsilon = 5.0 \times 10^4$ M^{-1} cm^{-1}). (B) UV−vis absorption spectra of MgPz in an ethanol solution (1) and on a 200 nm Ag film (2). The two spectra are arbitrarily scaled. Absorption maxima are located at 548 and 598 nm.

calculated as $A_{surf}(\lambda) = -\log(\text{sample}(\lambda)/\text{reference}(\lambda))$. All the measurements were conducted in air at room temperature.

Synthesis of Iron(II) Tris-2,2′-Bipyridine (Fe(bpy)$_3$[PF$_6$]$_2$). Fe-(bpy)$_3^{2+}$[PF$_6$]$_2$ (Fe(bpy)$_3^{2+}$) was synthesized according to Leidner et al.[30] In summary, a 1:3 mole ratio of Fe(NH$_4$)$_2$SO$_4 \cdot$6H$_2$O/2,2′-dipyridyl was added to water with stirring. This solution was heated at 80 °C for 1 h. An excess of NH$_4$PF$_6$ was added quickly, and the mixture was stirred for 2 min. The solution was allowed to cool. The resulting red precipitate (Fe(bpy)$_3$(PF$_6$)$_2$, 91% yield) was filtered and dried.

Results and Discussion

Structure and Electronic Absorption Spectrum of MgPz. Figure 2A shows the structure of MgPz. This molecule has D_{4h} symmetry and contains a magnesium-centered porphyrazinato ring that adsorbs parallel to a Ag surface with a thickness of ~0.4 nm, as determined by atomic force microscopy (AFM). The solution absorption spectrum of MgPz is shown in Figure 2B-1. The electronic spectrum contains two features that are

(30) Fussa-Rydel, O.; Zhang, H. T.; Hupp, J. T.; Leidner, C. R. *Inorg. Chem.* **1989**, *28*, 1533−1537.
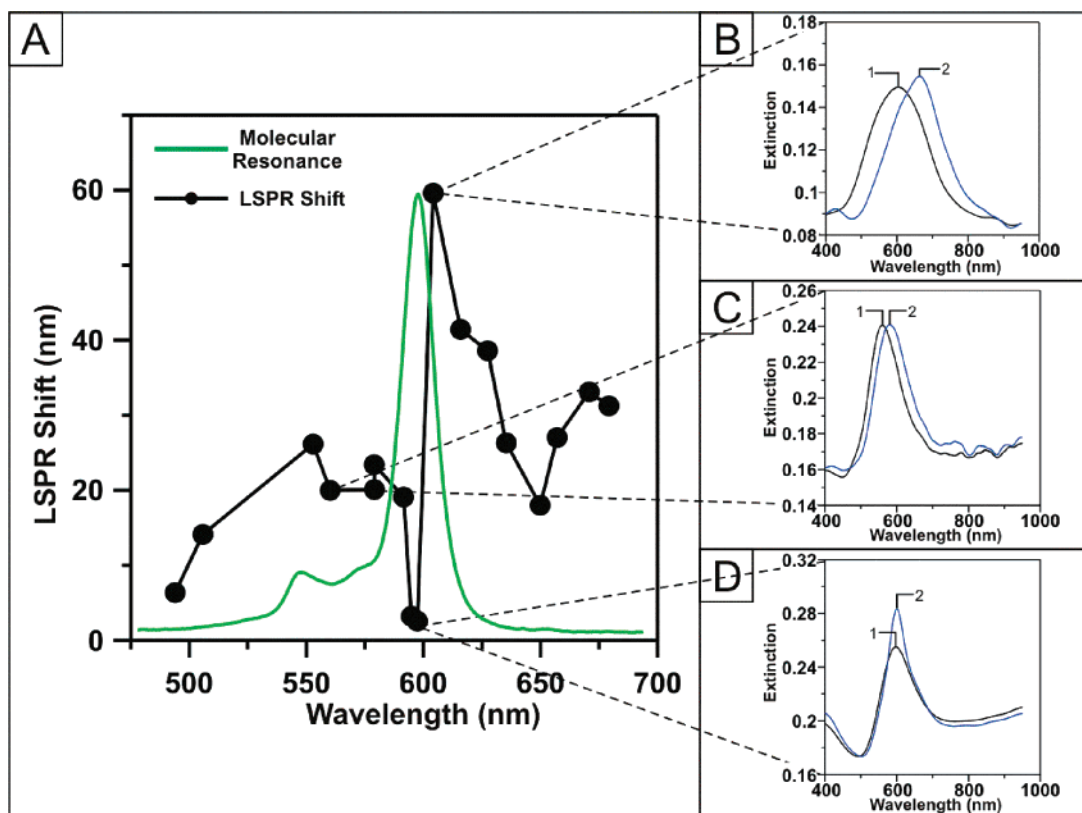
Figure 3. Influence of MgPz on the LSPR shift of Ag nanoparticles. (A) LSPR shift vs LSPR wavelength for the resonant adsorbate, MgPz. Solid black line with filled dots is a plot of the LSPR shift (nm) vs spectral position of Ag nanoparticles. The black dots represent the location of extinction maxima of bare Ag nanoparticles. The solid green line is the absorption spectrum of the adsorbate, MgPz (arbitrary scaling). (B) LSPR spectra of nanoparticles ($a = 118$ nm, $b = 55.0$ nm) in a N_2 environment. Ag nanoparticles (1) before chemical modification, $\lambda_{max} = 604.2$ nm, and (2) after modification with 50 μM MgPz, $\lambda_{max} = 663.8$ nm. The LSPR shift = 59.6 nm, %ΔFWHM = -22%, and %ΔI = $+12$%. (C) LSPR spectra of nanoparticles ($a = 90$ nm, $b = 55.0$ nm) in a N_2 environment. Ag nanoparticles (1) before chemical modification, $\lambda_{max} = 560.2$ nm, and (2) after modification with 50 μM MgPz, $\lambda_{max} = 580.2$ nm. The LSPR shift = 20.0 nm, %ΔFWHM = -3.2%, and %ΔI = 0.1%. (D) LSPR spectra of nanoparticles ($a = 90$ nm, $b = 60.0$ nm) in a N_2 environment. Ag nanoparticles (1) before chemical modification, $\lambda_{max} = 597.4$ nm and (2) after modification with 50 μM MgPz, $\lambda_{max} = 599.9$ nm. The LSPR shift = 2.5 nm, %ΔFWHM = -28.1%, and %ΔI = 34.0%.

both polarized within the plane of the molecule. We tentatively assign the peaks as a split Q-band ($\pi-\pi^*$ transition) with a strong low-energy absorbance centered at 598 nm ($\epsilon = 5 \times 10^4$ M^{-1} cm^{-1}; FWHM, $\Gamma = 704.6$ cm^{-1}, 25.61 nm) and a slightly higher energy shoulder at 548 nm.[31-34] Because of the narrow and simple electronic absorption and the large extinction coefficient of the molecule, MgPz presents a nearly ideal candidate for studying the interaction between an adsorbate-centered electronic transition and the nanoparticle-centered localized surface plasmon resonance.

To determine if adsorption of MgPz onto a silver surface influences that electronic spectrum of the molecule, we have measured the weak spectrum associated with MgPz adsorbed onto a polycrystalline silver film. As shown in Figure 2B-2, the surface spectrum is essentially identical to that in solution. Because the surface absorption spectrum of MgPz is not radically different than the solution absorption spectrum, we conclude that it is a reasonable approximation to use the solution data to compute the real and imaginary refractive index contributions with the Kramers–Kronig transformation.

(31) Montalban, A. G.; Lange, S. J.; Beall, L. S.; Mani, N. S.; Williams, D. J.; White, A. J. P.; Barrett, A. G. M.; Hoffman, B. M. *J. Org. Chem.* **1997**, *62*, 9284–9289.
(32) Velazquez, C. S.; Fox, G. A.; Broderick, W. E.; Andersen, K. A.; Anderson, O. P.; Barrett, A. G. M.; Hoffman, B. M. *J. Am. Chem. Soc.* **1992**, *114*, 7416–7424.
(33) Gouterman, M. *Porphyrins* **1978**, *3*, 1–165.
(34) Linstead, R. P.; Whalley, M. *J. Chem. Soc.* **1952**, 4839–4846.

Wavelength Dependence of the MgPz-Induced LSPR Shift. Nanoparticles with plasmon resonances that vary throughout the visible region of the spectrum were fabricated with NSL, and the effect of a monolayer of MgPz on the LSPR shift and line shape was monitored. Figure 3A reveals the influence of a monolayer of MgPz on the LSPR wavelength shift. The data points represent the LSPR of bare Ag nanoparticles with varied in-plane widths and out-of-plane heights. The electronic absorption spectrum of MgPz has been included for direct comparison to the experimental data points. Off molecular resonance, a LSPR shift of ~20 nm was observed, and no change in line shape was detected (Figure 3C). However, when nanoparticle plasmon resonances overlap with the molecular resonances, interesting behavior is revealed. When a LSPR peak maximum directly overlaps with a molecular resonance maximum, the LSPR shift drops sharply to less than 2 nm, and an apparent change in the peak shape of the LSPR is observed (Figure 3D). When the LSPR maximum is slightly red-shifted from the molecular resonance, the LSPR shift recovers and is amplified by 300% over the average LSPR shift (20 nm) to 60 nm (Figure 3B). As the peak position of the nanoparticle LSPR is further red-shifted from the molecular resonance, the LSPR shift slowly recovers to its average (20 nm). An added observable is the development of a small shoulder at ~630 nm. It is clear that the data do *not* track with the solution absorption spectrum but do exhibit wavelength-dependent LSPR shifts.

Empirical Model of Wavelength Shift. Previously, we have demonstrated that the LSPR wavelength shift ($\Delta\lambda_{max}$) can be predicted using the following equation:[10,12,13,35]

$$\Delta\lambda_{max} = m(n_{ads} - n_{N_2})(1 - e^{-2d/l_d}) \qquad (1)$$

where m is the refractive index sensitivity of the nanoparticles ($\sim$200 nm/RIU),[9,11] n_{ads} is the refractive index of the molecular adsorbate, n_{N_2} is the refractive index of the N_2 surroundings (1.0), d is the molecular thickness (experimentally determined to be 0.4 nm), and l_d is the characteristic electromagnetic field decay length of the nanoparticles (tunable but approximately 6 nm).[10] It is convenient to express n_{ads} as $n_{ads} = n_{non,ads} + \Delta n_{res,ads}$, where $n_{non,ads}$ is the nonresonant part of the refractive index and $\Delta n_{res,ads}$ is the resonant contribution. By solving eq 1 for n_{ads} and assuming the aforementioned values, the refractive index of the adsorbate layer can be estimated. Notice that the average $\Delta\lambda_{max}$ at off-molecular resonance wavelengths is 20 nm. The nonresonant average refractive index of the MgPz monolayer is calculated to be $\sim$2.0. When the nanoparticle LSPR and molecular resonances directly overlap, the refractive index of the adsorbate drops to a minimum of 1.02. At the maximum LSPR shift, the refractive index is estimated to be 3.38. While we are making many assumptions in this model, this clearly indicates that the effective refractive index of the MgPz monolayer, and therefore the LSPR shift response, is highly wavelength dependent.

As shown in Figure 3, the suppression and subsequent amplification of this response do not exactly follow the line shape of the free molecule (solution) electronic absorption spectrum. In an effort to understand these results, the electronic absorption spectrum of MgPz was transformed using the Kramers−Kronig equation. As indicated by the calculated refractive indices from eq 1, it was hypothesized that the wavelength-dependent LSPR shift data was influenced by the wavelength-dependent refractive index of the adsorbing monolayer. The Kramers−Kronig transformation[36] allows the extraction of the real component of the wavelength-dependent refractive index of the molecule from the imaginary portion of the spectrum or vice versa. Using this treatment,[37] the real part of the resonant component of the refractive index was calculated from the molecular absorption spectrum (the imaginary component of the refractive index) using the following equation:

$$\Delta n_{res,ads}(\omega') = \frac{c}{\pi} \int_0^\infty \frac{\Delta\alpha(\omega)}{\omega^2 - (\omega')^2} \, d\omega \qquad (2)$$

where $\Delta\alpha$ is the change in the absorption coefficient ($2.303A(\lambda)/T$, where $A(\lambda)$ is the molecular absorbance at a given wavelength and T is the effective molecular thickness), c is the speed of light, λ is the wavelength of light, and ω is the angular frequency ($2\pi c/\lambda$).

Figure 4A shows the LSPR shift predicted using eq 1, including a scaled version of the Kramers−Kronig estimate from eq 2. The DDA calculations were performed for truncated tetrahedron particle shapes in which the base and the height
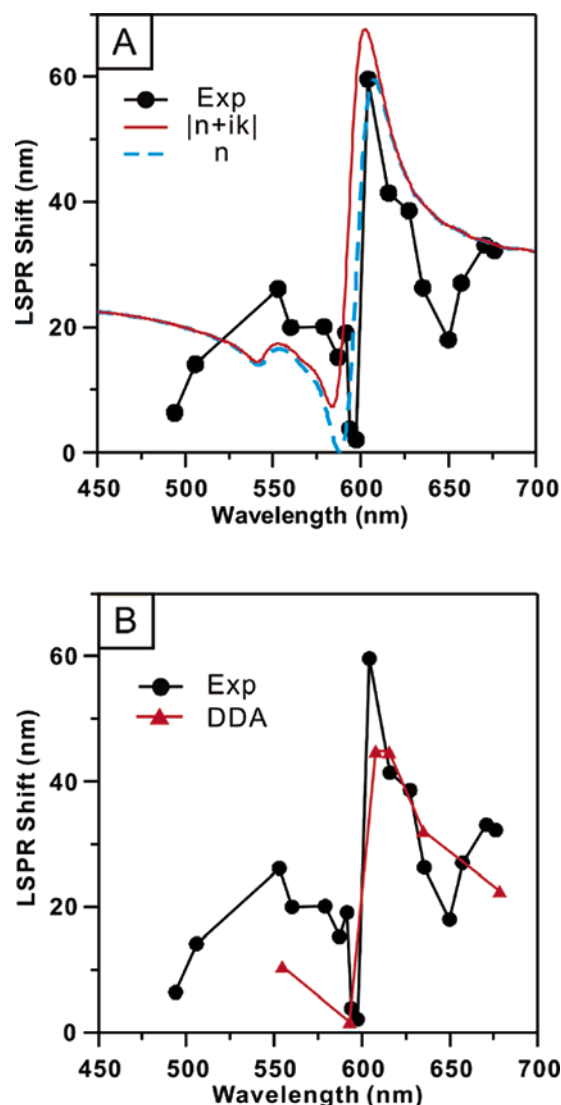
(35) Jung, L. S.; Campbell, C. T.; Chinowsky, T. M.; Mar, M. N.; Yee, S. S. *Langmuir* **1998**, *14*, 5636−5648.
(36) Kronig, R. d. L.; Kramers, H. A. *Z. Phys.* **1928**, *48*, 174−179.
(37) Schanze, K. S.; Bergstedt, T. S.; Hauser, B. T.; Cavalaheiro, C. S. P. *Langmuir* **2000**, *16*, 795−810.

Figure 4. Two theoretical models used to interpret the data. In each example, the solid black line with filled dots is a plot of the experimental LSPR shift (nm) vs spectral position of the Ag nanoparticles. (A) Predicted LSPR shift (using eq 1) using two semiempirical models with a scaled refractive index from Kramers−Kronig analysis. (B) Theoretical prediction of the LSPR shift using a scaled refractive index from Kramers−Kronig analysis (theoretical monolayer thickness of MgPz = 2 nm). The refractive index was scaled as $RI_{scaled} = (5n_{ads} + 2.0) + i5k_{ads}$.

were varied to vary the plasmon wavelength through the molecular resonance. The scale factor is chosen to be 5, based on visual fits of the empirical result to the measured data. It should be noted that, had we scaled the Kramers−Kronig result to the AFM thickness, the scale factor would have to be increased by an additional factor of $\sim$5. Also included is an estimate in which n_{ads} in eq 1 is replaced by the absolute magnitude of the refractive index, i.e., $(n_{ads}^2 + k_{ads}^2)^{1/2}$, where k_{ads} is the imaginary part of the refractive index, $k_{ads} = \Delta\alpha\lambda/4\pi$. Use of the absolute value is common in studies of dielectric effects on diffraction intensities;[38] however, it is less clear that this applies to plasmon wavelengths, and we include it simply for comparison purposes.

Figure 4A clearly shows that the scaled LSPR shift data using the real part of the refractive index track well with the

(38) Aizenberg, J.; Rogers, J. A.; Paul, K. E.; Whitesides, G. M. *Appl. Opt.* **1998**, *37*, 2145−2152.

transformed data, and better than data obtained using the absolute value of the refractive index. Without scaling, the Kramers−Kronig transformation of a solution absorption measurement predicts changes in the real portion of the refractive index between $-0.198 < \Delta n_{res,ads} < 0.276$, and thus a variation of LSPR peak shift (from eq 1) between $20.0 \leq \Delta\lambda_{max} \leq 31.8$ nm. However, the experimental data reveal a LSPR shift variation between $2 \leq \Delta\lambda_{max} \leq 60$ nm, so clearly scaling is important. This discrepancy between the Kramers−Kronig result and experiment can be understood on the basis of a surface-induced change in the absorption coefficient. Physically, this change can be understood since the adsorbate molecules should be aligned on the surface, whereas for the solution-phase measurement they will be randomly oriented. Alignment of the adsorbates could produce transition moments that are not orientation averaged, which should lead to an enhancement in effective absorption coefficient of roughly a factor of 3 (the inverse of the average of $\cos^2 \theta$). Additional enhancement in the absorption coefficient can arise from electronic coupling between the molecule and metal.

Electrodynamics Modeling of the LSPR Shift. In an attempt to understand these data more quantitatively, we have modeled the experimental results presented above using the discrete dipole approximation (DDA) method,[39,40] which is a finite element-based approach to solving Maxwell's equations for light interacting with an arbitrary shape/composition nanoparticle. Bare silver nanoparticles with a truncated tetrahedral shape were first constructed from cubical elements, and then one to two layers of the adsorbate were added to the exposed surfaces of the nanoparticle using the same elements. All calculations refer to silver nanoparticles with a dielectric constant taken from Lynch and Hunter.[41] Note that the dielectric constant is taken to be a local function, as there is no capability for a nonlocal description within the DDA approach. There have been several earlier studies in which the DDA method has been calibrated by comparison with experiment for truncated tetrahedral particles, including studies of external dielectric effects and substrate effects,[1,42,43] and on this basis we expect the DDA analysis to provide a useful qualitative description of the results.

The DDA grid size in these calculations is taken to be 1 nm, and the thickness of each monolayer in these studies is 2 nm. Unfortunately, it is not possible to use a grid size small enough to describe the layer more precisely. The refractive index of the layer is taken from the scaled Kramers−Kronig analysis, which means that the real part is determined by eq 2 multiplied by the scaling factor noted above and summed with the background value 2.0, and the imaginary part is given by k_{ads}, as given above multiplied by the scaling factor.[44]

Results from these calculations, along with the corresponding experimental data, are displayed in Figure 4B. The figure shows wavelength shifts that are similar to those obtained using eq 1 with the same scaled refractive index. This confirms that eq 1
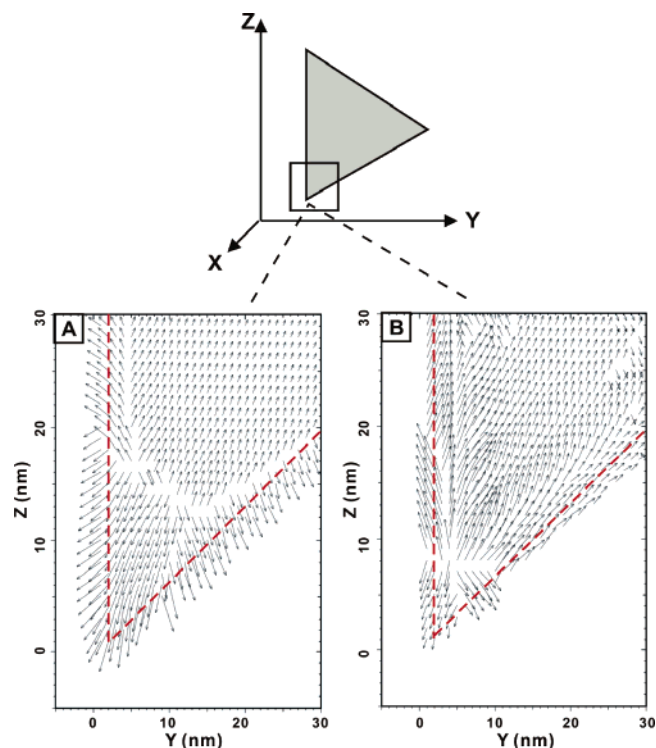
(39) Draine, B. T.; Flatau, P. J. *J. Opt. Soc. Am. A* **1994**, *11*, 1491−1499.
(40) Kelly, K. L.; Coronado, E.; Zhao, L.; Schatz, G. C. *J. Phys. Chem. B* **2003**, *107*, 668−677.
(41) Lynch, D. W.; Hunter, W. R. In *Handbook of Optical Constants of Solids*; Palik, E. D., Ed.; Academic Press: New York, 1985; pp 350−356.
(42) Jensen, T. R.; Kelly, K. L.; Lazarides, A.; Schatz, G. C. *J. Cluster Sci.* **1999**, *10*, 295−317.
(43) Jensen, T. R.; Schatz, G. C.; Van Duyne, R. P. *J. Phys. Chem. B* **1999**, *103*, 2394−2401.
(44) Born, M.; Wolf, E. *Principles of Optics: Electromagnetic Theory of Propagation, Interference and Diffraction of Light*, 6th ed.; Pergamon Press Inc.: Elmsford, NY, 1980.
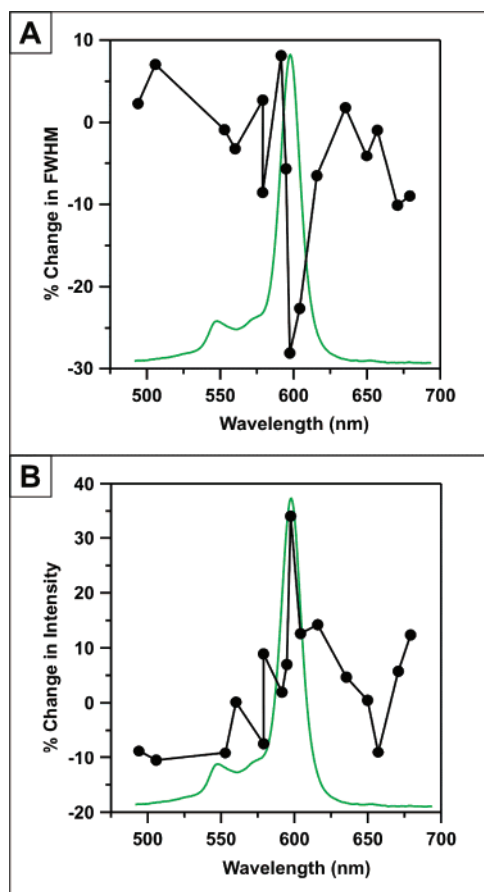
Figure 5. Induced polarizations for one tip at the bottom of a silver particle covered with a 2 nm layer of MgPz molecules in the $y-z$ plane at two different wavelengths. The silver particle is 104 nm wide (bisector) and 30 nm high. The polarization direction is along the z axis. The amplitude of each vector is the modulus of the complex polarization. Red dashed lines denote the edge of the silver particle, which means that polarization vectors above and to the right of the red lines are for silver and those outside the triangle (below or to the left) are for MgPz. (A) Results for $\lambda = 590$ nm. (B) Results for $\lambda = 620$ nm.

provides a useful empirical parametrization of the wavelength shift and, in particular, that the absolute value of the refractive index in eq 1 is not important. In addition, it shows that the previously derived scaling factor needs to be included in order to generate results that match the experimental results quantitatively.

The DDA results can be used to provide a qualitative picture that explains the wavelength dependence of the LSPR wavelength shift. Figure 5 presents a plot of the induced polarizations near one tip at the bottom of a silver particle that is covered with a 2 nm layer of MgPz molecules in the $y-z$ plane at two different wavelengths. The polarization direction is along the z axis, and the amplitude of each vector is determined by the modulus of the complex polarization. Red dashed lines denote the edge of the particle, which means that polarization vectors above and to the right of the red lines refer to silver and those below and to the left are for MgPz. Figure 5A shows results for a nanoparticle at $\lambda = 590$ nm (on the blue side of the molecular resonance associated with the minimum shift in Figure 3A). The molecular and metal polarizations are mostly in the opposite direction at this wavelength. Figure 5B shows results for the nanoparticle at $\lambda = 620$ nm (on the red side of the molecular resonance). At this wavelength, the polarization vectors are more strongly aligned with each other and with the polarization direction. This change in the direction of the induced polarization arises because of a change in the sign of the molecular polarizability as one tunes from the red side of the molecular resonance to the blue side. When the polarizations

Figure 6. Influence of MgPz on the FWHM and intensity of the LSPR of Ag nanoparticles. (A) Percent change in the FWHM of LSPR of Ag nanoparticles vs the spectral position of Ag nanoparticles (solid black line with filled dots). The black dots represent the location of the extinction maxima of bare Ag nanoparticles. The solid green line is the absorption spectrum of the adsorbate, MgPz (arbitrarily scaled). (B) Percent change in the intensity of the LSPR of Ag nanoparticles vs the spectral position of Ag nanoparticles (solid black line with filled dots). The black dots represent the location of the extinction maxima of bare Ag nanoparticles. The solid green line is the absorption spectrum of the adsorbate, MgPz (arbitrarily scaled).

are aligned, the wavelength shift is large, while when they are opposed, the shift is small. This effect has previously been noted by Wiederrecht et al. concerning the interaction of noble metal particles with excitons in J-aggregates, where a 100-fold decrease was observed in the exciton lifetime when the plasmon wavelength is tuned to the red of the exciton wavelength by switching from silver to gold.[45]

Influence of a Monolayer of MgPz on the LSPR Peak FWHM. In previous LSPR experiments, the FWHM (in eV) of the LSPR of the nanoparticles did not change after functionalization of their surfaces with molecules.[10,11] It should be noted, however, that the molecules studied did not have molecular resonances in the visible region of the spectrum that could overlap with the LSPR of the nanoparticles. For this reason, the FWHMs of the nanoparticle plasmon resonances were monitored and compared using the following equation:

$$\%\Delta FWHM = 100 \times \left(\frac{FWHM(eV)_{after} - FWHM(eV)_{before}}{FWHM(eV)_{before}} \right)$$
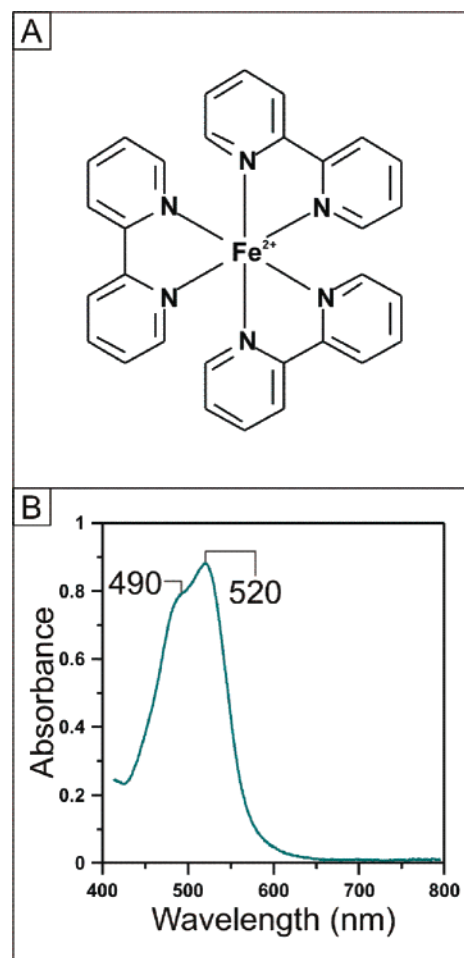
$$(3)$$

where %ΔFWHM is the percent change in the FWHM of the

Figure 7. Iron(II) trisbipyridine. (A) Structure of iron(II) trisbipyridine (Fe(bpy)$_3^{2+}$) (MW = 838.3 g/mol, $\epsilon = 8.6 \times 10^3$ M^{-1} cm^{-1} at 520 nm). (B) The electronic absorption spectrum of 100 μM Fe(bpy)$_3^{2+}$ in ethanol (path length, $b = 1.0$ cm). Absorption maxima are located at 490 and 520 nm.

LSPR, FWHM(eV)$_{after}$ is the FWHM of the plasmon peak after functionalization with the molecular adsorbate, and FWHM-(eV)$_{before}$ is the FWHM of the plasmon peak before functionalization with the molecular adsorbate.

Figure 6A displays the change in FWHM of the LSPR of Ag nanoparticles versus the spectral position of the Ag nanoparticles upon exposure to MgPz. It is shown that, when the LSPR is not coincident with the molecular resonance, the FWHM of the nanoparticles varies by only ±10%. When the LSPR is fabricated to overlap with the molecular resonance of MgPz, the FWHM of the LSPR narrows dramatically, by ~25% (from its original). While a slight narrowing of the LSPR is expected when the refractive index of the nanoparticles' dielectric surrounding is increased, the magnitude of the variation in refractive index calculated from the Kramers–Kronig analysis does not accurately predict this level of change.

Influence of a Monolayer of MgPz on the LSPR Peak Intensity. Similar to the FWHM comparison, the intensity of the LSPR peak, in general, does not vary upon the absorption of nonresonant molecules onto the surface of the nanoparticles.[12,13] As shown previously, the FWHM of the LSPR varies versus the spectral peak position of the Ag nanoparticles in

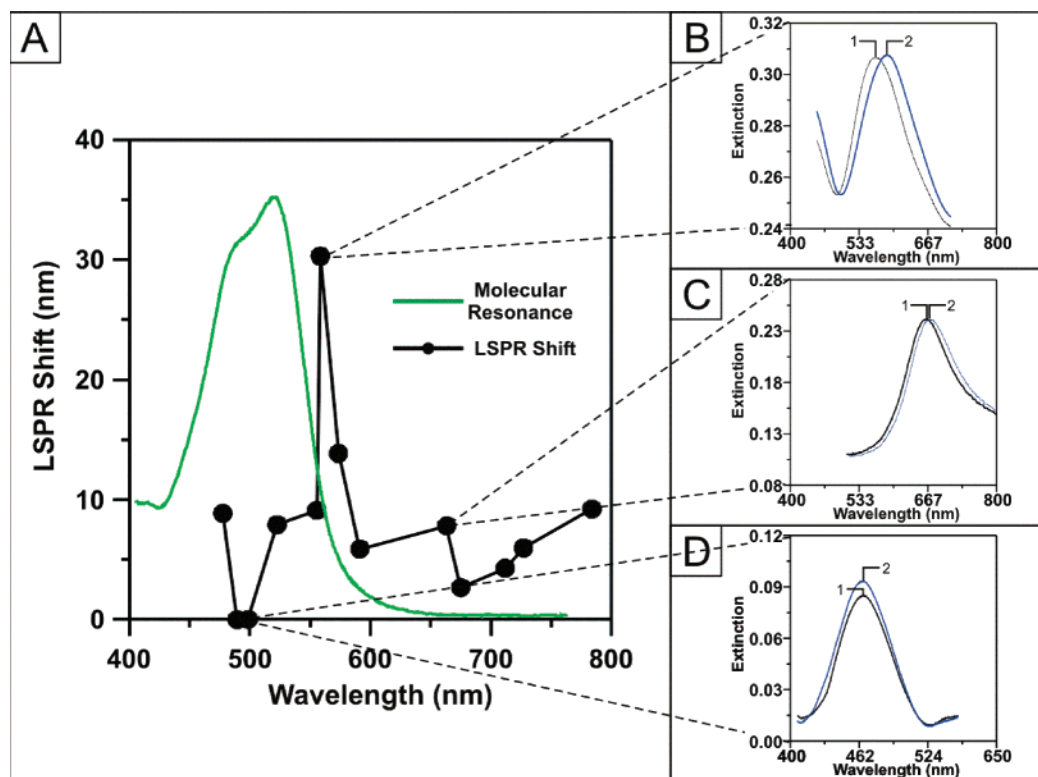(45) Wiederrecht, G. P.; Wurtz, G. A.; Hranisavljevic, J. *Nano Lett.* **2004**, *4*, 2121–2125.

Figure 8. Influence of $Fe(bpy)_3^{2+}$ on the LSPR shift of Ag nanoparticles. (A) LSPR shift vs LSPR wavelength for the resonant adsorbate, $Fe(bpy)_3^{2+}$. Solid black line with filled dots is a plot of the LSPR shift (nm) vs spectral position of Ag nanoparticles. The black dots represent the location of extinction maxima of bare Ag nanoparticles. The solid green line is the absorption spectrum of the adsorbate, $Fe(bpy)_3^{2+}$ (arbitrary scaling). (B) LSPR spectra of nanoparticles ($a = 72$ nm, $b = 40.0$ nm) in a N_2 environment. Ag nanoparticles (1) before chemical modification, $\lambda_{max} = 558.6$ nm, and (2) after modification with 100 μM $Fe(bpy)_3^{2+}$, $\lambda_{max} = 588.9$ nm. The LSPR shift = 30.3 nm, %ΔFWHM = -2.9%, and %ΔI = $+4.2$%. (C) LSPR spectra of nanoparticles ($a = 105$ nm, $b = 30.0$ nm) in a N_2 environment. Ag nanoparticles (1) before chemical modification, $\lambda_{max} = 663.2$ nm and (2) after modification with 100 μM $Fe(bpy)_3^{2+}$, $\lambda_{max} = 671.0$ nm. The LSPR shift = 7.8 nm, %ΔFWHM = $+1.3$%, and %ΔI = $+2.3$%. (D) LSPR spectra of nanoparticles ($a = 72$ nm, $b = 38.0$ nm) in a N_2 environment. Ag nanoparticles (1) before chemical modification, $\lambda_{max} = 489.4$ nm and (2) after modification with 100 μM $Fe(bpy)_3^{2+}$, $\lambda_{max} = 489.4$ nm. The LSPR shift = 0.0 nm, %ΔFWHM = $+4.5$%, and %ΔI = $+6.4$%.

comparison to the molecular resonance. For this reason, we analyzed intensity changes in the LSPR versus the LSPR spectral position using the following equation:

$$\%\Delta I = 100 \times \left(\frac{I_{after} - I_{before}}{I_{before}}\right) \quad (4)$$

where %ΔI is the percent change in the intensity of the LSPR, I_{after} is the intensity of the plasmon peak after functionalization with the molecular adsorbate, and I_{before} is the intensity of the plasmon peak before functionalization with the molecular adsorbate. As shown in Figure 6B, when the LSPR is offset from the molecular resonance, the intensity of the LSPR peak decreases slightly or remains at its average. A large increase in the plasmon intensity is observed when the plasmon peak directly overlaps with the molecular resonance.

It is apparent from these studies with MgPz that the wavelength variation in refractive index, as calculated using the Kramers−Kronig analysis, does not predict a large enough influence on the LSPR shift, FWHM variations, and intensity changes. For this reason, we chose to study a second molecular system to ascertain the generality of the MgPz results.

Structure and Electronic Absorption Spectrum of Fe-(bpy)$_3^{2+}$. To verify that the trends observed with MgPz are seen with other molecules, a second molecule, $Fe(bpy)_3^{2+}$ (Figure 7A), was studied. $Fe(bpy)_3^{2+}$ binds irreversibly to Ag with a thickness of ~1.3−1.4 nm, as determined by AFM (data not

shown). Because the crystal structure of $Fe(bpy)_3^{2+}$ indicates a largest dimension of 1.3 nm,[46] the AFM measurements are consistent with a monolayer of material on the nanoparticle surface. This molecule, with D_{3d} symmetry, has two electronic resonances in the visible region of the spectrum (Figure 7B). There is a voluminous literature concerning the assignment of these bands. The consensus view is that these molecular resonances are assigned to two electronic transitions that are polarized in different orientations.[47,48] The primary transition is located at 520 nm and has an extinction coefficient of 8600 M^{-1} cm^{-1}.[49] The second transition appears as a shoulder at 490 nm, with an extinction coefficient of 7700 M^{-1} cm^{-1}.[49]

Wavelength Dependence of the Fe(bpy)$_3^{2+}$-Induced LSPR Shift. Similar to the approach taken with the MgPz experiments, nanoparticles with plasmon resonances that vary throughout the visible region of the spectrum were fabricated with NSL, and the effects of a monolayer of $Fe(bpy)_3^{2+}$ on the LSPR shift and line shape were monitored. Figure 8A reveals the influence of a monolayer of $Fe(bpy)_3^{2+}$ on the LSPR wavelength shift. The data points represent the LSPR of bare Ag nanoparticles with varied in-plane widths and out-of-plane heights. Off molecular resonance, a LSPR shift of ~8 nm was observed and no change

(46) Dick, S. Z. *Kristallogr., New Crys. Struct.* **1998**, *213*, 356.
(47) Felix, F.; Ferguson, J.; Guedel, H. U.; Ludi, A. *Chem. Phys. Lett.* **1979**, *62*, 153−157.
(48) Decurtins, S.; Felix, F.; Ferguson, J.; Guedel, H. U.; Ludi, A. *J. Am. Chem. Soc.* **1980**, *102*, 4102−4106.
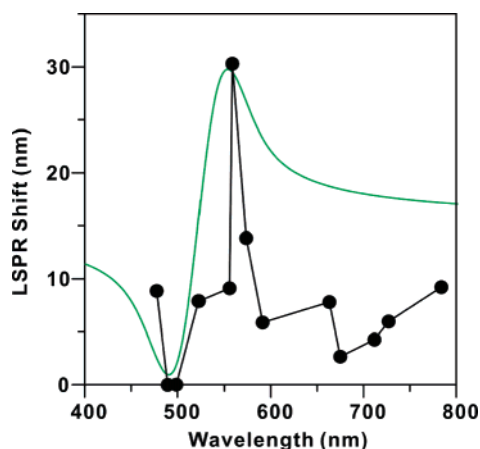(49) Hanazaki, I.; Nagakura, S. **1969**, *8*, 648−653.

Figure 9. Data interpretation using Kramers−Kronig analysis. LSPR shift vs LSPR wavelength for the resonant adsorbate, $Fe(bpy)_3^{2+}$. Solid black line with filled dots is a plot of the LSPR shift (nm) vs spectral position of Ag nanoparticles. The black dots represent the location of extinction maxima of bare Ag nanoparticles. The solid green line is the predicted LSPR shift using the semiempirical model (the real part of refractive index) with a scaled refractive index from Kramers−Kronig analysis. The estimation of the refractive index was scaled as $RI_{scaled} = (7n_{ads} + 1.2) + i7k_{ads}$.

in line shape was detected (Figure 8C). It should be noted that this LSPR shift is ∼2 times smaller than the off-resonance shift from the MgPz response. While $Fe(bpy)_3^{2+}$ has a larger molecular weight and forms a thicker layer on the nanoparticle surfaces, its effective refractive index is smaller than that of MgPz. This is a result of the inherently large void volume of $Fe(bpy)_3^{2+}$ caused by the steric hindrance of its large bipyridine rings in the molecule.

Figure 8 shows that, when the nanoparticle plasmon resonance overlaps with the molecular resonance spectrum, the LSPR shift enhancement is observed for only one of the two electronic transitions. When the LSPR maximum directly overlaps with the bluer molecular resonance maximum, the LSPR shift drops sharply to less than 1 nm (Figure 8D). When the nanoparticle plasmon resonance is fabricated to overlap with the molecular resonance at 520 nm, the LSPR shift appears to be unaffected by the presence of the overlapping molecular resonance. When the LSPR maximum is slightly red-shifted from the molecular resonance, the LSPR shift recovers and is amplified by 3 times over the average LSPR shift to 30 nm (Figure 8B). As the peak position of the nanoparticle LSPR is further red-shifted from the molecular resonance, the LSPR shift recovers to its average.

To test our earlier modeling based on eq 1, the solution absorption spectrum was analyzed via the Kramers−Kronig analysis, and the resulting real portion of the refractive index was used in eq 1 with scaling by a factor of 7 (Figure 9). The Kramers−Kronig analysis in this case was based only on fits to the 520 nm absorption peak. Once again, the scaled refractive index roughly matches the observed wavelength-dependent variation in the LSPR shift response. The absence of structure arising from the state at 490 nm suggests that the transition moment associated with this transition is parallel to the surface and thus does not couple significantly to the local electromagnetic field.

Influence of a Monolayer of $Fe(bpy)_3^{2+}$ on the LSPR Peak FWHM. As demonstrated with the MgPz molecule, the FWHM (in eV) of the LSPR of the nanoparticles narrows when the electronic transition of the molecule resonance overlaps with the plasmon resonance. Because $Fe(bpy)_3^{2+}$ appears to display

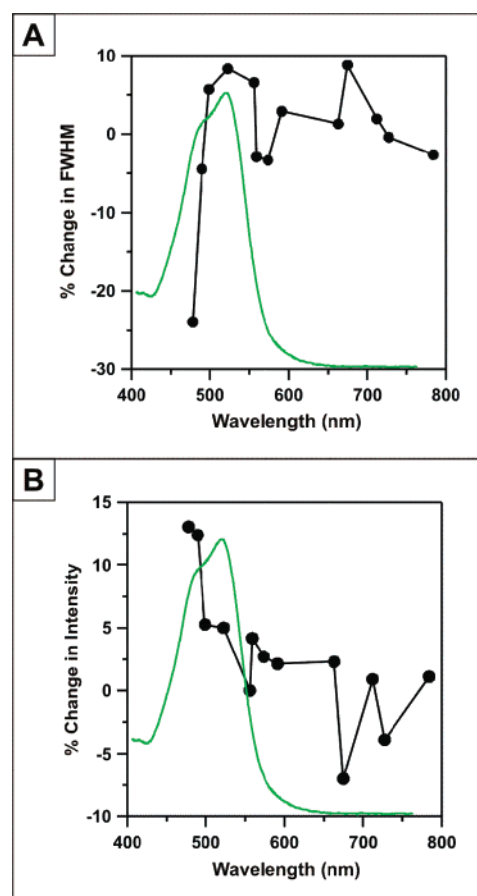**Figure 10.** Influence of $Fe(bpy)_3^{2+}$ on the FWHM and intensity of the LSPR of Ag nanoparticles. (A) Percent change in the FWHM of LSPR of Ag nanoparticles vs the spectral position of Ag nanoparticles (solid black line with filled dots). The black dots represent the location of the extinction maxima of bare Ag nanoparticles. The solid green line is the absorption spectrum of the adsorbate, $Fe(bpy)_3^{2+}$ (arbitrarily scaled). (B) Percent change in the intensity of the LSPR of Ag nanoparticles vs the spectral position of Ag nanoparticles (solid black line with filled dots). The black dots represent the location of the extinction maxima of bare Ag nanoparticles. The solid green line is the absorption spectrum of the adsorbate, $Fe(bpy)_3^{2+}$ (arbitrarily scaled).

a dependence of the LSPR shifts on the nature of the electronic transitions, changes in the FWHM of the plasmon were monitored and compared using eq 3. Surprisingly, electronic transition dependence exists in these data, also (Figure 10A). When the nanoparticle LSPR overlaps with the molecular transition at 490 nm, behavior similar to that of the MgPz molecule is observed: the FWHM narrows upon exposure to a monolayer of $Fe(bpy)_3^{2+}$. Due to instrumental limitations of the spectrometer and the difficulty in fabricating samples with LSPR extinction maxima less than ∼460 nm, no data were collected blue of this peak. When the nanoparticle LSPR maximum is increased to overlap with the molecular transition at 520 nm, the FWHM of the LSPR remains relatively unchanged. This behavior continues for all other plasmon spectral peak positions.

Influence of a Monolayer of $Fe(bpy)_3^{2+}$ on the LSPR Peak Intensity. In the MgPz experiments, the LSPR peak intensity appeared to increase when the molecular resonance directly overlapped with the plasmon resonance. Once again, $Fe(bpy)_3^{2+}$ displays mode selectivity associated with the particular molecular transition (Figure 10B). When the LSPR of the nanoparticles is coincident with the electronic transition at 490 nm, the peak intensifies by ∼13%. At all other spectral positions, including

the molecular transition at 520 nm, the peak intensity varies between ±5%. It should be noted that this molecular transition dependence is opposite to that observed in Figure 9, where the transition at 490 nm seems to be coupling strongly to the nanoparticle resonance and the transition at 520 nm is not.

Conclusions

The results presented here systematically probe the effect that molecular electronic resonances have on the intensity, FWHM, and LSPR wavelength shift of the plasmon resonance of Ag nanoparticles. By systematically tuning the LSPR extinction maxima of Ag nanoparticles versus the wavelength position of the molecular electronic resonances, new phenomena are revealed. First, the LSPR peak shift induced by a resonant molecule has an oscillatory dependence on wavelength. While the trends in these data qualitatively track with the Kramers−Kronig transformation of the molecular resonance spectrum (real portion of the refractive index) for the MgPz molecule, the magnitude of the response is underestimated. This was verified both in empirical model calculations based on eq 1 and in the DDA calculations, and it suggests that the molecular absorption intensity is enhanced by surface adsorption.

When the molecular system was changed to $Fe(bpy)_3^{2+}$, it was revealed that the enhanced LSPR shifts, plasmon narrowing, and intensification occurred for only one of the two electronic transitions in the visible molecular spectrum. If the variation in these data were caused only by the wavelength-dependent refractive index changes induced by the molecular transitions

(as implied with the Kramers−Kronig transformation), no transition dependence would be observed. From this observation and from the change in LSPR peak shape upon absorption of a monolayer of the resonant molecules on resonance-matched LSPR peak maxima, we hypothesize that the nanoparticle plasmon resonance and molecular resonances are coupling energetically and that the polarization of the molecular resonances plays an important role in this interaction. Of course, it is also possible that the transition moments are altered by adsorption, and this, combined with adsorbate-induced shifts in molecular resonance wavelengths and changes in adsorbate widths, means that the simple Kramers−Kronig model has important limitations for describing these experiments. Future experiments will concentrate on determining this interaction and the electronic structure of the absorbed species more precisely. These results will have implications in molecular-enhanced LSPR sensing and in the understanding of all surface-enhanced spectroscopies (including surface-enhanced resonance Raman spectroscopy).

JA063575Q